

Article

Comparison of Acid- and Base-Modified Biochar Derived from Douglas Fir for Removal of Copper (II) from Wastewater

Beatrice Arwenyo ^{1,2}, Prashan M. Rodrigo ¹, Olalekan A. Olabode ^{1,3}, Hashani P. Abeyasinghe ¹,
Jessie N. Tisdale ¹, Rose C. Azuba ⁴ and Todd E. Mlsna ^{1,*}

¹ Department of Chemistry, Mississippi State University, Starkville, MS 39762, USA; b.arwenyo@gu.ac.ug (B.A.); pmr161@msstate.edu (P.M.R.); oao59@msstate.edu (O.A.O.); ha600@msstate.edu (H.P.A.); jessietisdale@yahoo.com (J.N.T.)

² Department of Chemistry, Gulu University, Gulu P.O. Box 166, Uganda

³ Department of Pure and Applied Chemistry, Osun State University, Osogbo 230212, Osun State, Nigeria

⁴ College of Veterinary Medicine, Animal Resources and Biosecurity, Makerere University, Kampala P.O. Box 7062, Uganda; roseazuba@gmail.com

* Correspondence: tmlsna@chemistry.msstate.edu; Tel.: +1-662-325-6744; Fax: +1-662-325-1618

Abstract: Copper is a non-biodegradable heavy metal, and high levels in water bodies cause serious environmental and health issues. Douglas fir biochar has a higher number of carboxylic, phenolic, and lactonic groups, which provide suitable active sites for copper removal. Douglas fir biochar (BC) was modified using 20% solutions of KOH (KOH/BC), H₂SO₄ (H₂SO₄/BC), and Na₂CO₃ (Na₂CO₃/BC). All materials were characterized using SEM, SEM-EDS, FTIR, TGA, XRD, BET, and elemental analysis. These modifications were done to compare the activations of those sites by measuring copper removal efficiencies. KOH/BC, H₂SO₄/BC, and Na₂CO₃/BC materials gave surface areas of 389.3, 326.7, and 367.9 m² g⁻¹, respectively, compared with pristine biochar with a surface area of 578.9 m² g⁻¹. The maximum Langmuir adsorption capacities for Na₂CO₃/BC, KOH/BC, BC, and H₂SO₄/BC were 24.79, 18.31, 17.38, and 9.17 mg g⁻¹, respectively. All three modifications gave faster kinetics at 2 mg/L initial copper concentrations (pH 5) compared with pristine BC. The copper removal efficiency was demonstrated in four different spiked real water matrices. The copper removals of all four water matrices were above 90% at 2 mg/L initial concentration with a 2 g/L biochar dosage. The competitive effects of Pb²⁺, Zn²⁺, Cd²⁺, and Mg²⁺ were studied at equimolar concentrations of Cu²⁺ and competitive ions for all four materials.

Keywords: modified biochar; wastewater; copper; adsorbents



Citation: Arwenyo, B.; Rodrigo, P.M.; Olabode, O.A.; Abeyasinghe, H.P.; Tisdale, J.N.; Azuba, R.C.; Mlsna, T.E. Comparison of Acid- and Base-Modified Biochar Derived from Douglas Fir for Removal of Copper (II) from Wastewater. *Separations* **2024**, *11*, 78. <https://doi.org/10.3390/separations11030078>

Academic Editor: Anastasia D. Pournara

Received: 22 January 2024

Revised: 22 February 2024

Accepted: 26 February 2024

Published: 1 March 2024



Copyright: © 2024 by the authors. Licensee MDPI, Basel, Switzerland. This article is an open access article distributed under the terms and conditions of the Creative Commons Attribution (CC BY) license (<https://creativecommons.org/licenses/by/4.0/>).

1. Introduction

Heavy metal presence in water remains a critical pollution problem across the globe. Even at low concentrations, heavy metals accumulate in the environment and can be transferred to humans from plants and animals via the food chain [1]. These non-degradable metals are toxic and have serious health risks. Copper, though essential to both plants and animals at low concentrations [2,3], causes anemia, kidney damage, stomach and intestinal distress, coma, and eventual death if the threshold limit is exceeded [4,5]. Continuous copper accumulation in the environment results from human activities, including industrialization, waste from copper mines, and poor waste management of copper-containing materials such as from electric wires, analytical reagents, and electroplating [6]. The United States Environment Protection Agency has recommended maximum drinking water copper concentration limits of 1.3 mg L⁻¹ [7,8].

Various treatment methods, including ion exchange, precipitation, adsorption, and solvent extraction, have been used for heavy metal removal from aqueous solutions [9,10]. However, technologies such as ion exchange, precipitation, and solvent extraction not only create other problems such as metal-bearing sludge, but are costly [11]. Adsorption is a

relatively inexpensive treatment method. This, however, depends on the adsorbents used. Activated carbon, biochar, and clay are some of the common adsorbents used for water treatment [7,12]. Both activated carbon and biochar are characterized by large surface areas and surface functional groups that aid the removal of contaminants. Compared with activated carbon, biochar is less expensive and easier to make [10]. In addition, biochar adsorption ability can be further improved by modification [13].

Recently, interest in developing low-cost and eco-friendly adsorbents has grown. Different cheap adsorbents have been used to remove metal ions from wastewater, including pine fruit [14], wheat straw, rice hulls and lentil shells [15], peat, marine algae, clays, maize cob, bagasse, and palm fruit bunch. Pavan Kumar et al. used groundnut seed cake, sesame seed cake, and coconut seed cake powders as biosorbents to remove Cu^{2+} from an aqueous solution and attained maximum adsorption capacities of 4.82, 4.24, and 4.32 mg g^{-1} , respectively [16]. Shah et al. reported a maximum Cu^{2+} adsorption capacity of 28.75 mg/g from an aqueous solution using a copolymer obtained by grafting cassava starch with 5-chloromethyl-8-hydroxyquinoline [5]. Information regarding commercially available adsorbents, including Douglas fir biochar, is currently limited and lacks comprehensive documentation.

In this work, the use of commercially available Douglas fir biochar was investigated as an economical and available adsorbent to remove copper from aqueous solutions. Douglas fir biochar is a byproduct of syngas production by Biochar Supreme Company. Our major focus was to investigate the effects of post-treatment on Douglas fir biochar Cu^{2+} sorption capacity. Moreover, we focused on activating lactones, phenols, and carboxylic groups present in Douglas fir biochar using acid and base modifications [17]. Different treatment reagents, including KOH, Na_2CO_3 , and H_2SO_4 , were used for the post-treatment. Several characterization studies, including SEM, EDX, XRD, and TGA, were performed.

2. Materials and Methods

2.1. Chemicals

Analytical grade materials, including (KOH ($\geq 85\%$), NaOH ($\geq 97\%$), Na_2CO_3 ($\geq 99.5\%$), HCl ($\sim 37\%$), H_2SO_4 (95–98%), HNO_3 ($\sim 70\%$), $\text{CuSO}_4 \cdot 5\text{H}_2\text{O}$ ($\geq 98\%$), $\text{Pb}(\text{NO}_3)_2$ ($\geq 99\%$), $\text{Zn}(\text{NO}_3)_2 \cdot 6\text{H}_2\text{O}$ ($\geq 98\%$), $\text{Mg}(\text{NO}_3)_2 \cdot 6\text{H}_2\text{O}$ ($\geq 99\%$), $\text{Cd}(\text{NO}_3)_2 \cdot 4\text{H}_2\text{O}$ ($\geq 98\%$), and NaCl ($\geq 99\%$), were purchased from Sigma Aldrich (Saint Louis, MO, USA).

2.2. Preparation of Douglas Fir Biochar

Douglas fir biochar (BC) is obtained as a byproduct from bio-syngas production. It is a commercial product (Black Owl Biochar Environment Ultra) from Biochar Supreme Inc. (Everson, WA, USA) The biochar preparation method involved the introduction of green Douglas fir wood chips into an air-fed updraft wood gasifier at ~ 900 – 1000 °C for a residence time of ~ 10 – 30 s. This method was previously reported by Bombuwala et al. [18].

2.3. Modification of Douglas Fir Biochar (BC)

Douglas fir biochar (BC) of particle size ≤ 420 μm was treated with 20% solutions of KOH, H_2SO_4 , and Na_2CO_3 , respectively, with 20 g of Douglas fir biochar mixed with 100 mL of each solution and the slurry stirred for 24 h with a magnetic stirrer at a speed of 400 rpm at ~ 25 °C. After standing for another 24 h, the supernatant was filtered through Whatman No. 1 filter paper using a vacuum filter, and the residues were washed three times each with 200 mL of deionized water (DI H_2O) before oven-drying (105 °C) to a constant weight. The untreated and KOH-, H_2SO_4 -, and Na_2CO_3 -treated Douglas fir biochar was designated as BC, KOH/BC, H_2SO_4 /BC, and Na_2CO_3 /BC, respectively.

2.4. Characterization of Douglas Fir Biochar and Modified Douglas Fir Biochar

The surface area and pore size analyses of the BC, KOH/BC, H_2SO_4 /BC, and Na_2CO_3 /BC were carried out based on the BET (Brunauer, Emmet, and Teller) method using N_2 at 77.30 K with a Micromeritics Tristar II Plus Version 2.03 Plus surface area analyzer. Prior

to the analysis, the samples were degassed for at least 6 h at 180 °C. The morphology of the samples was analyzed with scanning electron microscopy (JEOL JSM-6500F FE-SEM (Peabody, MA, USA) operated at 5 kV) and the mineral content was determined using scanning electron microscopy-electron diffraction energy (SEM-EDX) spectroscopy and Powder X-ray diffraction techniques (Rigaku Ultima III qualx 2.0 software with POWcod database), with an X-ray diffraction system using Cu-K α ($\lambda = 1.54 \text{ \AA}$) radiation at 45 kV and 40 mA. The XRD patterns were measured by scanning 2θ from 0° to 90° at 4° min⁻¹.

Fourier transform infrared spectroscopy (FT-IR) analysis of Douglas fir biochar and activated Douglas fir biochar was performed using a Nicolet 6700 FT-IR spectrometer (Thermo Fisher Scientific, Inc., Waltham, MA USA) fitted with an attenuated total reflectance (ATR) accessory. FTIR spectra for 400 scans with 8 cm⁻¹ resolution were obtained in the wavenumber range of 500–4000 cm⁻¹.

Thermogravimetric analysis (TGA) of biochar samples was carried out using a TGA Q50 V20.13 Build 39 analyzer (TA instrument, New Castle, DE, USA). The biochar was heated from ambient temperature to 1000 °C at a heating rate of 10 °C/min. The instrument was programmed to ramp at 10 °C/min from ambient temperature to 30 °C in nitrogen (N₂) at a flow rate of 50 mL min⁻¹, hold at 30 °C for 5 min, then rise from 30 to 1000 °C. The derivative of the thermogravimetry curves (DTG, wt. %/min) was calculated by differentiating the TGA (wt. %) data.

2.5. PH Point of Zero Charge (pH_{pzc})

The solution pH at which the net surface charge on the absorbent BC, KOH/BC, H₂SO₄/BC, and Na₂CO₃/BC is zero (pH_{pzc}) was determined by adding 25 mL of 0.01 M NaCl solution to each sample (~50 mg) placed in a 50 mL polypropylene tube [19,20]. This was followed by agitating the mixture (rpm = 200) for 24 h at 25 °C. The resultant supernatant was filtered through Whatman no. 1 filter paper. The final pH of the filtrates was measured using a Hanna pH meter for the initial pH values of 0.7, 3.3, 5.1, 7.5, 9.0, 11.2, and 13.1. The solution pH was adjusted to the desired pH values using either 10 M NaOH or 10 M HCl solutions. Then, ΔpH (initial-final pH) values were plotted against the initial solution pH from which the pH_{pzc} was obtained.

2.6. Sorption of Copper onto BC, KOH/BC, Na₂CO₃/BC, and H₂SO₄/BC

A 1000 mg L⁻¹ Cu²⁺ stock solution was prepared by dissolving 3.96 g of (CuSO₄·5H₂O) 99% and diluting to 1 L with DI water. Working solutions of various concentrations were prepared from the stock solution after appropriate dilutions.

2.6.1. Effect of Initial pH on Copper Sorption onto KOH/BC, Na₂CO₃/BC, and H₂SO₄/BC

The study of the effect of initial solution pH values on copper adsorption was performed by adding 25 mL of 250 mg L⁻¹ Cu²⁺ solution to 50 mg of each adsorbent placed into a 50 mL polypropylene tube. The initial solution pH values were adjusted to 1, 2, 3, 4, 5, and 6 using either 0.1 M NaOH or 0.1 M HNO₃. Then, samples were agitated for 3 h at 25 °C. The supernatant was then filtered through Whatman no. 1 filter paper. The concentration of copper remaining in the filtrates was obtained using an Atomic Absorption Spectrometer SHIMADZU AA7000 (Kyoto, Japan) at a wavelength of 222.6 nm. The percentage of copper adsorbed was calculated from

$$\% \text{ Cu}^{2+} \text{ absorbed} = \frac{(C_o - C_f)}{C_o} \times 100\%$$

where C_o and C_f are the initial and final solution Cu²⁺ concentrations.

The pH and electrical conductivity of the filtrates were determined using a Hanna pH meter and electrical conductivity meters.

2.6.2. Adsorption Kinetic

The kinetics study was carried out at room temperature. To 50 mg of each biochar sample placed in a 50 mL polypropylene tube, 25 mL of 2 mg L⁻¹ Cu²⁺ solution was added. Then, these mixtures were shaken for a predetermined time interval (5–360 min) at 200 rpm. The mixtures were then filtered through Whatman no. 1 filter paper, and the filtrates Cu²⁺ concentrations were analyzed using ICP-MS (model ELAN DRC II).

2.6.3. Adsorption Isotherm

The adsorption isotherm was obtained using a copper concentration range of 2–250 mg L⁻¹ at pH 5. To 50 mg of adsorbent placed in a 50 mL polypropylene tube, 25 mL of each solution was added, followed by 3 h agitation at 200 rpm at 25 °C. The suspensions were then filtered through Whatman no.1 filter paper and the filtrate copper concentrations were determined as described in Section 2.6.1. The copper amount adsorbed (q_e ; mg g⁻¹) was obtained from the expression below [21,22].

$$q_e = \frac{(C_i - C_e) \times V}{w}$$

where C_i and C_e are the initial and equilibrium concentrations of copper in the solution. V is solution volume (L) and w is the mass of adsorbent (g).

Langmuir adsorption capacities were calculated from the equation below [23].

$$q_e = \frac{q_{max} K_L C_e}{1 + K_L C_e}$$

where q_{max} , K_L , and C_e are the maximum adsorption capacity, Langmuir constant, and equilibrium concentration, respectively.

2.6.4. Real Lake Water Sample Study

Three water sources—Bluff Lake (33.283072, -88.776972), Briar Lake (33.432870, -88.767551), and Loakfoma Lake (33.263047, -88.778497)—were used to test the effectiveness of Cu²⁺ adsorption from real contaminated lake water onto BC, KOH/BC, Na₂CO₃/BC, and H₂SO₄/BC. Each water sample was spiked to make 2 mg L⁻¹ Cu²⁺, and 25 mL of each spiked water sample was added to 50 mg of BC, KOH/BC, Na₂CO₃/BC, and H₂SO₄/BC placed in a 50 mL polypropylene tube. The mixtures were shaken at 300 rpm for 3 h at room temperature, then filtered through Whatman no. 1 filter paper. The filtrates were analyzed for Cu²⁺ concentrations, as in Section 2.6.1.

3. Results and Discussion

3.1. Surface Area, Pore Volume, and Pore Size Diameter

Regardless of the treatment reagent, the surface area decreased upon modifying BC with 20% KOH (KOH/BC), 20% H₂SO₄ (H₂SO₄/BC), and 20% (Na₂CO₃/BC) solutions (Table 1).

Table 1. Surface area, pore volume, and pore size diameter of BC, KOH/BC, Na₂CO₃/BC, and H₂SO₄/BC.

Material ^a	BET Surface Area (m ² /g)	Pore Volume (cm ³ /g)	Pore Diameter (Å)
BC	578.90 ± 3.21	0.066	4.55
KOH/BC	389.30 ± 0.39	0.129	13.26
H ₂ SO ₄ /BC	326.65 ± 0.34	0.106	12.99
Na ₂ CO ₃ /BC	367.92 ± 3.44	0.127	13.76

^a BC = untreated Douglas fir biochar, KOH/BC = BC treated with 20% KOH, H₂SO₄/BC = BC treated with 20% H₂SO₄, and Na₂CO₃/BC = BC treated with 20% Na₂CO₃ solution.

In contrast, both the pore size volume and pore diameter increased after modifying BC to KOH/BC, H₂SO₄/BC, and Na₂CO₃/BC. The largest reduction in surface area (578.9 to 326.7 m²/g) was attained after modifying BC with 20% H₂SO₄ solution. The reduction in surface area following treatment with 20% KOH and 20% Na₂CO₃ solutions was from 578.9 to 389.3 and 367.9 m² g⁻¹, respectively. The BET nitrogen adsorption curves (Figure 1) indicated BC exhibited a type I isotherm before and after modifying to KOH/BC, Na₂CO₃/BC, and H₂SO₄/BC. Type I isotherm is often associated with the formation of micropores.

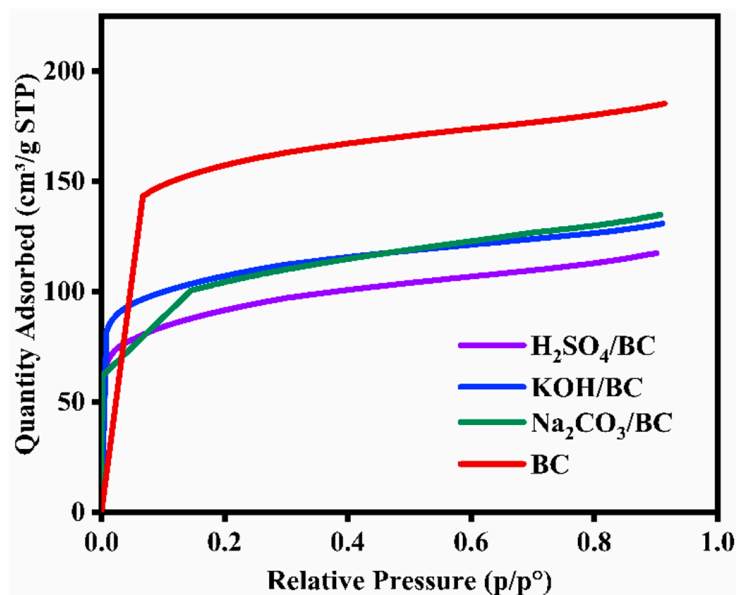


Figure 1. N₂ adsorption at 77.3 K of Douglas fir biochar (BC), BC treated with KOH (KOH/BC), BC treated with H₂SO₄ (H₂SO₄/BC), and BC treated with Na₂CO₃ (Na₂CO₃/BC).

The nitrogen adsorption capacities of BC, KOH/BC, Na₂CO₃/BC, and H₂SO₄/BC rose rapidly at relative pressure between 0 and 0.2 p/p^o. The rise in adsorption capacities at low relative pressure is attributed to monolayer adsorption. The small slopes exhibited between relative pressures of 0.2 and 0.9 could be due to multilayer adsorption. These results agree with those reported after modifying rice straw biochar with H₂SO₄ and HNO₃. The surface area reduction is caused by micropore destruction by modifying agents creating additional meso- and macropore fractions.

3.2. Surface Morphology and Elemental Compositions

The scanning electron microscopy (SEM) micrographs of BC, KOH/BC, H₂SO₄/BC, and Na₂CO₃/BC are shown in Figure 2. BC surface morphology changed after being modified to KOH/BC, H₂SO₄/BC, and Na₂CO₃/BC. After modification, the biochar pore structure appeared more developed and fragmented. Before treatment, BC had a smooth surface whose pores were hardly observed. After KOH and Na₂CO₃ treatment, the carbon material surface developed large pores. However, the H₂SO₄-treated biochar resulted in the collapse of the pore structure, lowering the surface area. The collapse of the pore structure is most likely due to corrosion by the acid. This observation is consistent with the BET surface area analysis results (Table 1 and Figure 1), indicating a lowering of the surface area. The collapse of the pore structure is most likely due to corrosion by the acid. This observation is consistent with the BET surface area analysis results (Table 1 and Figure 1).

The X-ray energy dispersion spectroscopy (EDS) results are shown in Figure 3. Pt was used as the coating material for the biochar during the analysis. As expected, the presence of elements was largely dependent on the treatment material.

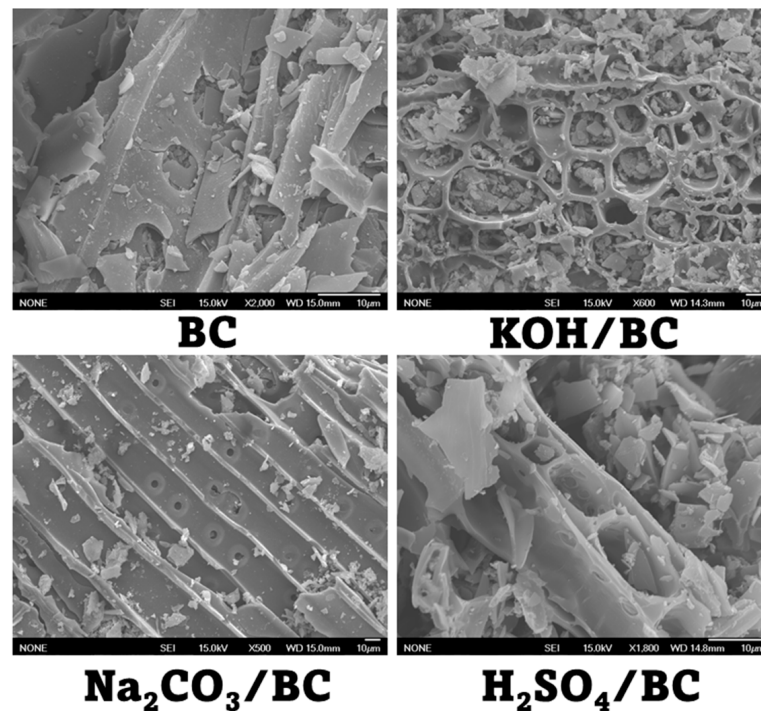


Figure 2. SEM micrographs showing surface morphology for BC, KOH/BC, Na₂CO₃/BC, and H₂SO₄/BC.

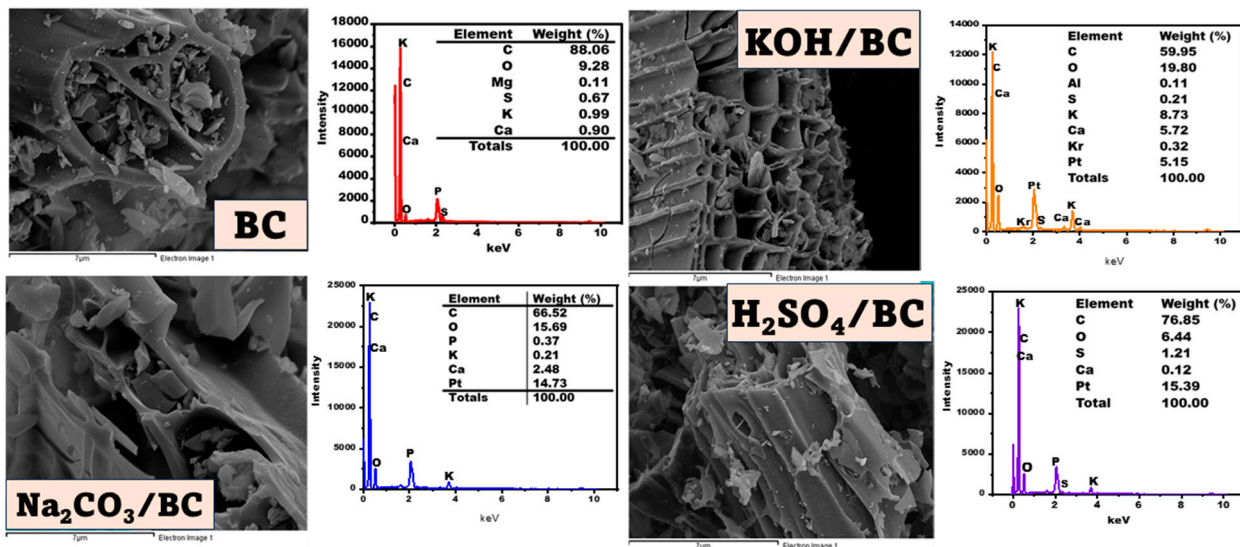


Figure 3. SEM-EDX images and elemental compositions for BC, KOH/BC, Na₂CO₃/BC, and H₂SO₄/BC.

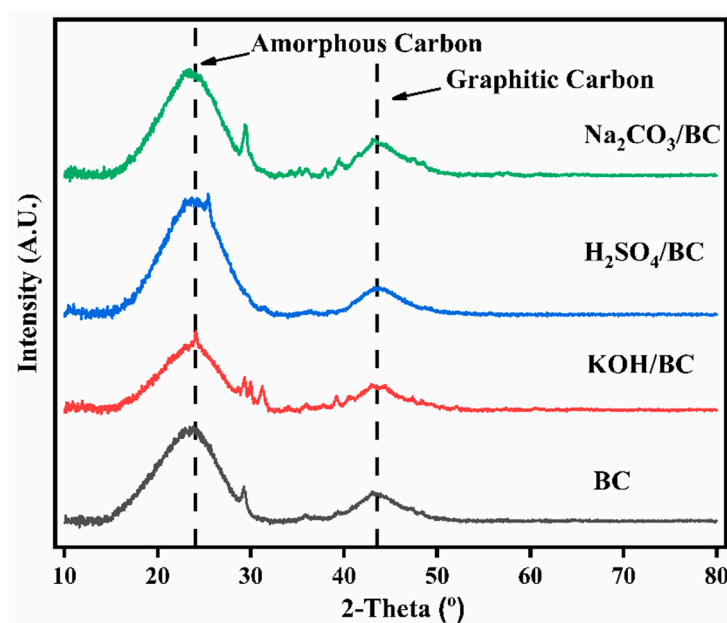
The chemical components of biochar were greatly altered upon modifying BC to KOH/BC, Na₂CO₃/BC, and H₂SO₄/BC. The %C decreased from ~92.3% in BC to ~81.6%, ~87.6%, and ~76.4% in KOH/BC, Na₂CO₃/BC, and H₂SO₄/BC, respectively. In contrast, the %O rose from ~4.8% in BC to ~11.0%, ~6.8%, and ~16.1% in KOH/BC, Na₂CO₃/BC, and H₂SO₄/BC, respectively (Table 2).

Table 2. Elemental compositions and ash contents of BC, KOH/BC, H₂SO₄/BC, and Na₂CO₃/BC.

Material	C [%]	H [%]	O [%]	N [%]	S [%]	Ash [%]
BC	92.29 ± 1.32	0.69 ± 0.01	4.75	0.13 ± 0.01	0.02 ± 0.00	2.13 ± 0.54
KOH/BC	81.62 ± 0.45	1.04 ± 0.03	10.98	0.2 ± 0.04	0.01 ± 0.01	6.15 ± 0.85
H ₂ SO ₄ /BC	76.39 ± 2.45	1.32 ± 0.05	16.08	0.25 ± 0.02	3.62 ± 0.80	1.89 ± 0.28
Na ₂ CO ₃ /BC	87.64 ± 0.87	0.83 ± 0.06	6.82	0.14 ± 0.07	0.05 ± 0.02	4.52 ± 0.49

3.3. XRD Analysis

The X-ray diffraction patterns of BC, KOH/BC, H₂SO₄/BC, and Na₂CO₃/BC are shown in Figure 4.

**Figure 4.** XRD patterns of BC, KOH/BC, H₂SO₄/BC, and Na₂CO₃/BC.

Generally, two broad peaks appeared at $2\theta = \sim 23.0^\circ$ and $\sim 43.4^\circ$, like those of amorphous and graphitic carbon, respectively [24]. These peaks correspond to the (002) and (100) carbon material crystal planes. The crystallinity of BC was $\sim 21.6\%$. The crystallinity of Na₂CO₃ and KOH-modified BC increased to $\sim 24.7\%$ and $\sim 27.5\%$, respectively, after the modifications. However, the crystallinity of H₂SO₄-modified BC was reduced to $\sim 19.6\%$ due to the collapse of pore structures inside the biochar matrix. The macroscopic carbon structure amorphousness can be attributed to low graphitization at the activation conditions [25].

3.4. FTIR Analysis

Figure S1 shows the FTIR spectra of BC, KOH/BC, Na₂CO₃/BC, and H₂SO₄/BC. The broad bands at wavenumbers 3500–4000 cm⁻¹ and 2818–2981 cm⁻¹ are attributed to the –OH stretching vibration of water and –CH₂ asymmetric stretching vibrations, respectively [26]. The peak between 975 and 750 cm⁻¹ is ascribed to out-of-plane aromatic C–H bending vibration [27]. The bands between 1040 and 1090 cm⁻¹ are due to the C–O stretching from the formation of singly bonded C–O moieties in lactones and phenols [28]. The peaks from 1861 to 1675 cm⁻¹ and 1405 to 1300 cm⁻¹ are attributed to aromatic C=C stretching and C–H deformation, respectively, in lignin [29]. After modifying BC to KOH/BC, Na₂CO₃/BC, and H₂SO₄/BC, both –OH and –CH₂ aliphatic bands decreased. These declines in –OH and –CH₂ bands might have resulted from the dehydration and deterioration in polar functional groups, respectively.

3.5. Thermogravimetric Analysis

Figure S2 shows the TGA curves for BC, KOH/BC, Na₂CO₃/BC, and H₂SO₄/BC. The biochars had varied degrees of thermal stability. In all cases, the first weight loss occurred between 50 and 100 °C, with weight losses of approximately 4.1, 3.0, 1.4, and 3.1% for BC, KOH/BC, Na₂CO₃/BC, and H₂SO₄/BC, respectively. These weight losses are attributed to the desorption of physically bound moisture. A gradual weight loss of ~34.4% occurred in KOH/BC between 250 and 1000 °C. The weight losses of BC, Na₂CO₃/BC, and H₂SO₄/BC are ~5.4, ~6.3, and ~4.6%, respectively, occurring between 250 and 600 °C, due to the pyrolysis of cellulose, hemicellulose, and portion of lignin. The final weight loss occurred between 650 and 1000 °C for BC (~10.2%), Na₂CO₃/BC (~2.0%), and H₂SO₄/BC (~12.6%). This weight loss at elevated temperatures is attributed to biomass thermo-oxidative degradation, such as lignin and inorganic material decomposition.

3.6. The point of Zero Charge (pH_{pzc})

The pH_{pzc} values for BC before and after modification to KOH/BC, Na₂CO₃/BC, and H₂SO₄/BC are shown in Figure 5.

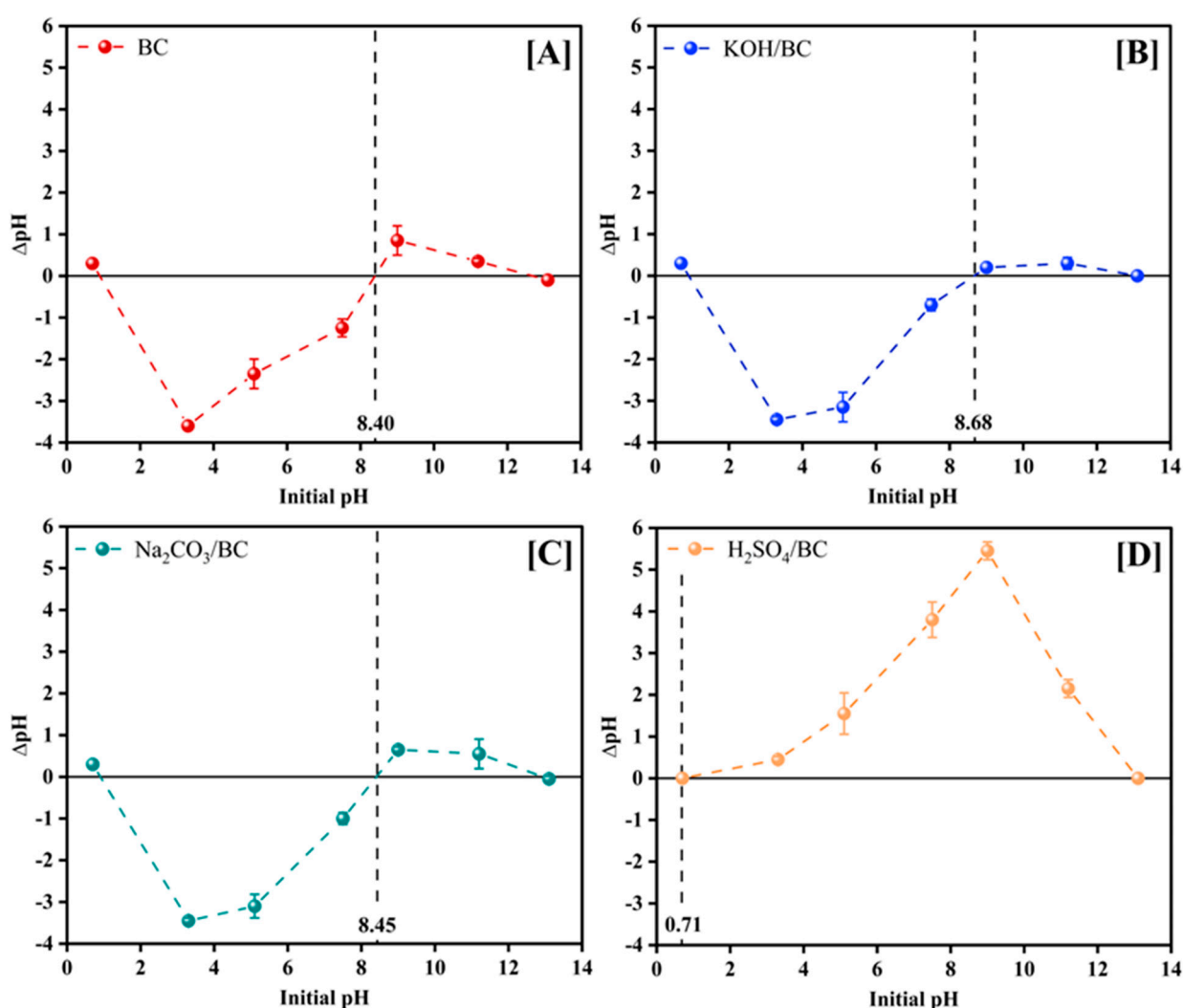


Figure 5. pH point of zero charge (pH_{pzc}) for (A) BC, (B) 20% KOH (KOH/BC), (C) 20% Na₂CO₃ (Na₂CO₃/BC), and (D) 20% H₂SO₄ (H₂SO₄/BC) materials. ΔpH was calculated as $\Delta pH = \text{Initial pH} - \text{Final pH}$.

The pH_{pzc} defines the pH value at which the adsorbent net surface charge equals zero. When $pH > pH_{pzc}$, the adsorbent surface is negatively charged, and adsorption of

cationic species is favored. At solution pH < p_{H_{PZC}}, the adsorbent surface is positively charged, which makes the adsorption of anions such as PO₄³⁻ on it favorable. The pristine biochar (BC) had a p_{H_{PZC}} of 8.40, which increased to 8.68 and 8.45 with modification to KOH/BC and Na₂CO₃/BC, respectively. However, the p_{H_{PZC}} decreased to 0.71 upon H₂SO₄ modification. During pyrolysis with KOH, the lactonic, carboxylic, and phenolic groups present are converted to negatively charged carboxylate and phenolate species, capable of releasing hydroxyl ions when in contact with water. However, in the presence of Na₂CO₃, only carboxylic and phenolic groups transform into their deprotonated species, resulting in lower basicity during the hydrolysis of water. But in the presence of H₂SO₄, most functional groups become protonated and release H⁺ into the medium upon contact with water.

3.7. Effects of Initial Solution pH

A pH dependence study was carried out between pH 1 and 6 because Cu²⁺ begins to precipitate at Cu(OH)₂ above pH 6 (Figure 6A). Figure 6 shows the adsorption capacities of Cu²⁺ on BC, KOH/BC, Na₂CO₃/BC, and H₂SO₄/BC as a function of the initial solution pH.

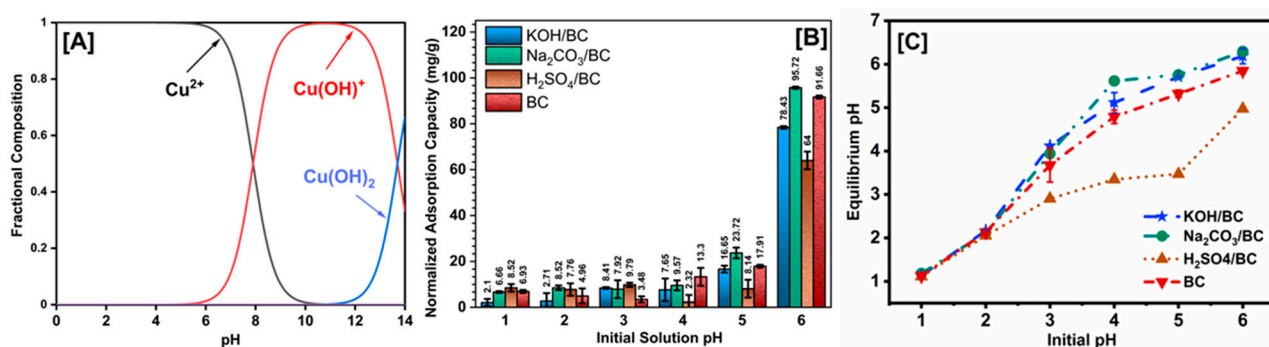


Figure 6. (A) Fractional composition of Cu²⁺ and (B) adsorption capacities of Cu²⁺ onto BC, BC treatment with 20% KOH (KOH/BC), BC treatment with 20% Na₂CO₃ (Na₂CO₃/BC), and BC treatment with 20% H₂SO₄ (H₂SO₄/BC) as a function of initial solution pH, and (C) equilibrium pH.

The highest sorption capacities of 95.72 ± 0.47, 91.66 ± 0.62, 78.43 ± 0.54, and 64.00 ± 3.88 mg/g corresponded to Na₂CO₃/BC, BC, KOH/BC, and H₂SO₄/BC, respectively, at pH 6. This is due to increased precipitation of Cu(OH)₂ at pH 6. Moreover, at the higher pH, deprotonation of carboxylic groups to carboxylate groups occurs, which can also increase the capacity of Cu²⁺. As expected, the results indicate low adsorption at low solution pH because Cu²⁺ competes with H⁺ for binding sites on the adsorbent surface. Moreover, at low pH values, pH < p_{H_{PZC}}, and the overall adsorbent surface becomes positively charged, which can repel the positively charged Cu²⁺ ions, thereby reducing adsorption. The results indicate low adsorption at lower solution pH values.

The plot of equilibrium pH measured after adsorption vs. the solution's initial pH is shown in Figure 6C. For highly acidic solutions (pH < 3), little or no difference in pH was observed after adsorption. At these pH values, Cu²⁺ adsorption onto the adsorbents was low (Figure 6C). Since pH did not increase, it is unlikely that hydrogen ion was released from the adsorbents; thus, the mechanism for adsorption at this pH does not act as a strong cation exchanger. The low absorption could have resulted from physisorption or chemisorption.

For initial solution pH values (pH > 3), the equilibrium solution pH values were less acidic for BC, KOH/BC, and Na₂CO₃/BC (Figure 6C). In contrast, the equilibrium solutions' pH tended to become more acidic after modification with H₂SO₄/BC due to the release of H⁺. For BC, KOH/BC, and Na₂CO₃/BC, the increase in solution pH is likely attributed to the release of OH⁻, which increases Cu²⁺ uptake. For H₂SO₄/BC, the H⁺ released when Cu²⁺ binds to it remains in the solution, resulting in a pH decrease. This observation also suggests that cation exchange is likely to be the adsorption mechanism at

these pH ranges. For H₂SO₄/BC, the H⁺ ion released when Cu²⁺ binds to it remains in the solution, resulting in a pH decrease.

3.8. Effect of Contact Time and Isotherm Study on Cu²⁺ Sorption onto BC, KOH/BC, Na₂CO₃/BC, and H₂SO₄/BC

Results for the effect of equilibrium time on Cu²⁺ sorption onto BC, KOH/BC, Na₂CO₃/BC, and H₂SO₄/BC are shown in Figure 7. Cu²⁺ adsorption onto the biochars was relatively fast (≤30 min).

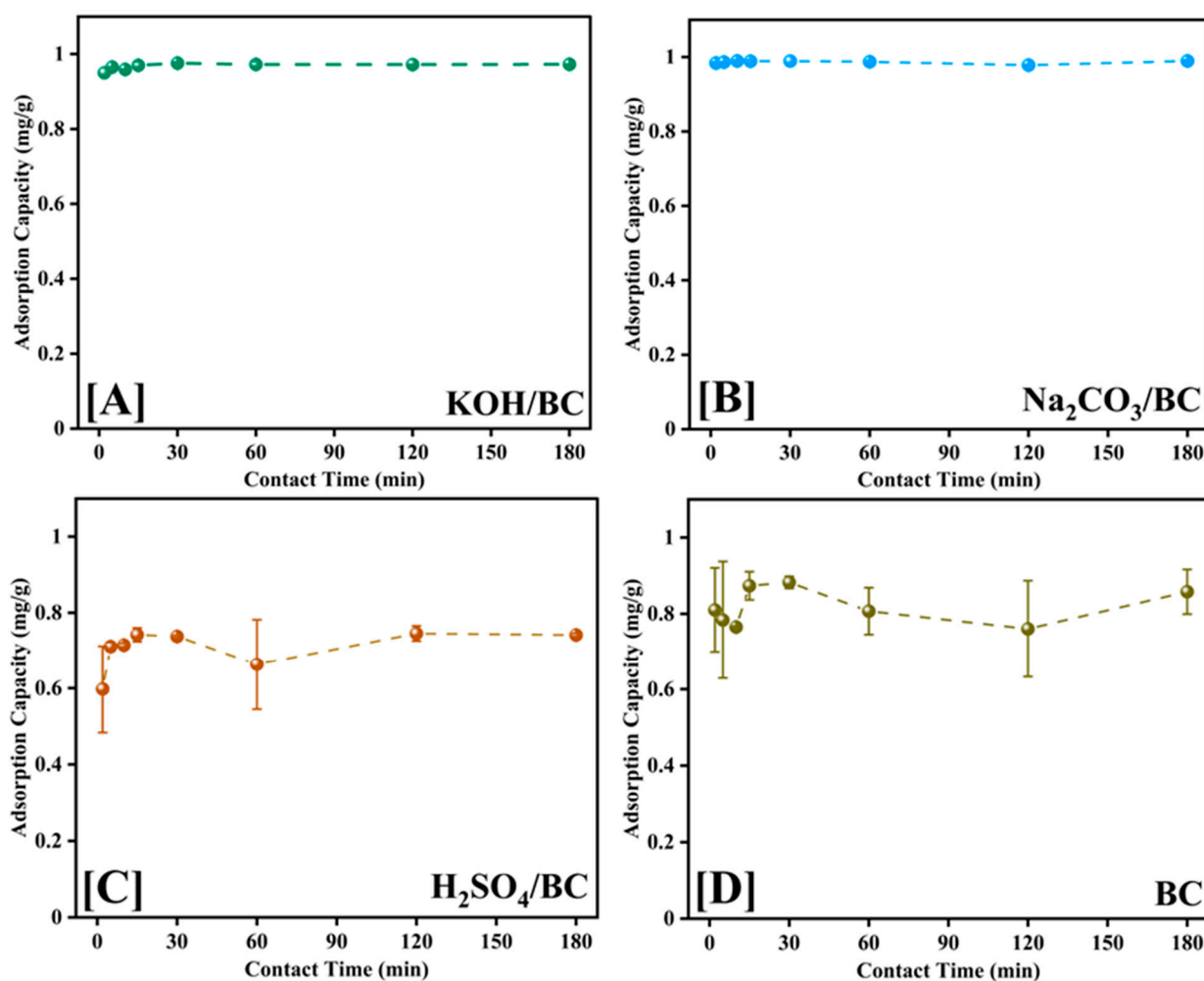


Figure 7. The effect of contact time on Cu²⁺ sorption onto (A) KOH/BC, (B) Na₂CO₃/BC, (C) H₂SO₄/BC, and (D) BC (at 25 °C and pH 5).

The fast ion uptake by the biochars might be ascribed to their large surface area for Cu²⁺ sorption onto the binding sites. Regardless of the adsorbent, Cu²⁺ removal rose with increased contact time. Further contact time increases, however, did not improve Cu²⁺ uptake, due to the saturation of the available adsorbent material’s adsorption sites.

Cu²⁺ sorption capacities onto BC, KOH/BC, Na₂CO₃/BC, and H₂SO₄/BC studied at pH 5 and 25 °C are presented in Figure 8A–D. Cu²⁺ removal capacities increased with initial solution Cu²⁺ concentrations.

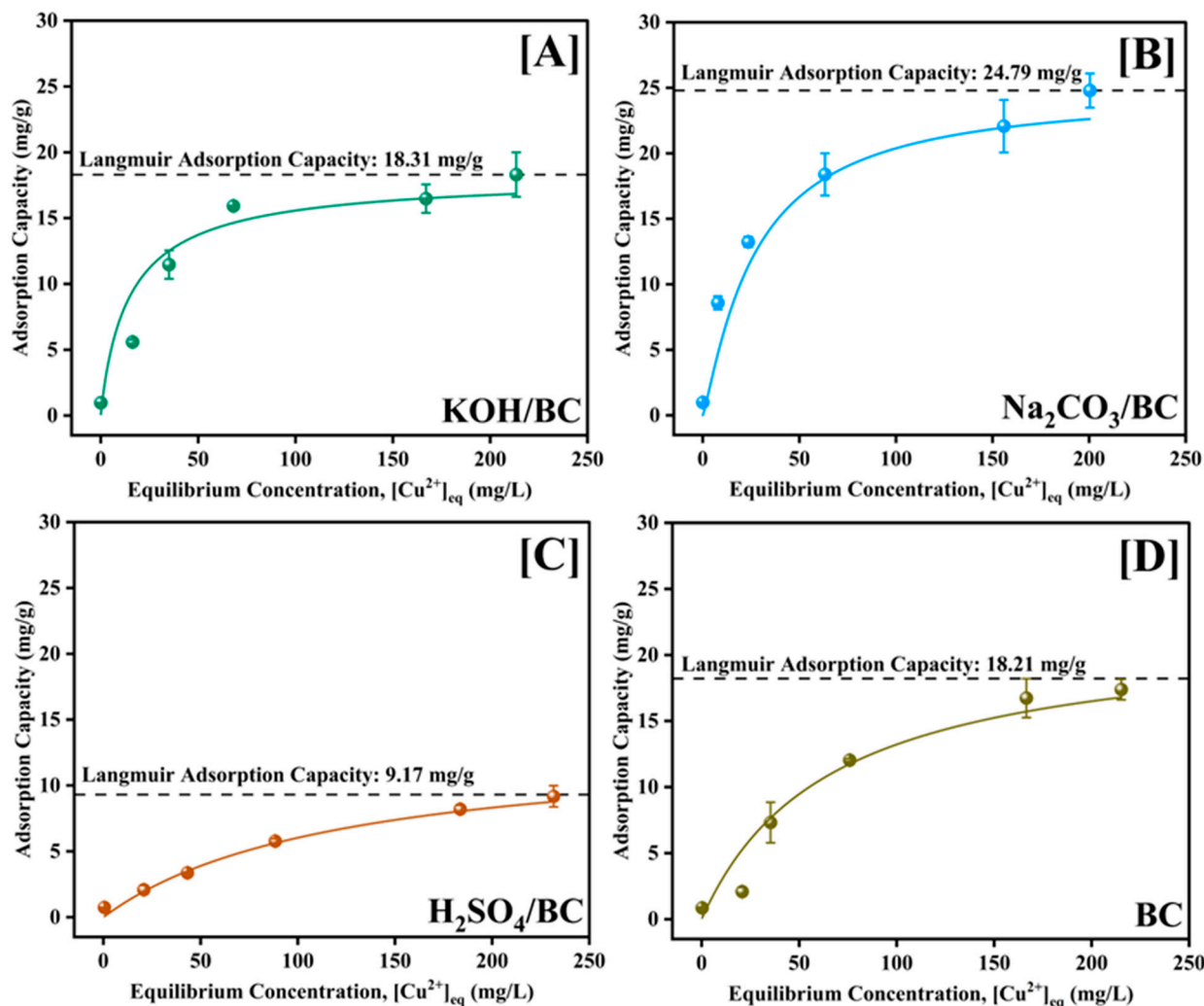


Figure 8. Cu^{2+} sorption capacities and non-linear Langmuir fits on KOH/BC (A), $\text{Na}_2\text{CO}_3/\text{BC}$ (B), $\text{H}_2\text{SO}_4/\text{BC}$ (C), and BC (D) at pH 5 and 25 °C.

The maximum Langmuir adsorption capacities were 18.31, 24.79, 9.17, and 18.21 mg g^{-1} for, KOH/BC, $\text{Na}_2\text{CO}_3/\text{BC}$, $\text{H}_2\text{SO}_4/\text{BC}$, and BC, respectively. The adsorption isotherm fits well to the two-parameter Langmuir model, with correlation coefficients of 0.92, 0.95, 0.99, and 0.93, respectively for KOH/BC, $\text{Na}_2\text{CO}_3/\text{BC}$, $\text{H}_2\text{SO}_4/\text{BC}$, and BC.

3.9. Effect of Competitive Ions

The competitiveness of ions depends on the pH, concentration, and ionic strength of the medium. This competitiveness for Cu^{2+} was studied using lead, zinc, cadmium, and magnesium ions. Equimolar concentrations (0.7 mM) of Cu^{2+} and competitive ions were studied at pH 5 (Figure 9).

Cu^{2+} showed adsorption capacities of 0.34 ± 0.01 , 0.33 ± 0.01 , 0.01 ± 0.00 , and 0.25 ± 0.12 mmol/g for KOH/BC, $\text{Na}_2\text{CO}_3/\text{BC}$, $\text{H}_2\text{SO}_4/\text{BC}$, and BC, respectively, with no competitive ion. In the presence of Pb^{2+} , Cu^{2+} showed capacities of 0.19 ± 0.01 , 0.18 ± 0.00 , 0.03 ± 0.00 , and 0.14 ± 0.02 mmol/g, respectively, for KOH/BC, $\text{Na}_2\text{CO}_3/\text{BC}$, $\text{H}_2\text{SO}_4/\text{BC}$, and BC. Pb^{2+} gave higher selectivity compared with Cu^{2+} due to the formation of $\text{Pb}(\text{OH})_2$ on biochar surfaces. This occurred because $\text{Pb}(\text{OH})_2$ precipitates at a lower pH than $\text{Cu}(\text{OH})_2$ [30]. Compared with Zn^{2+} , Cd^{2+} , and Mg^{2+} , all four biochar variants were more selective towards Cu^{2+} . In KOH/BC, the selectivity of the competitive ions increased in the order of $\text{Zn}^{2+} < \text{Cd}^{2+} < \text{Mg}^{2+}$. However, in BC, $\text{Na}_2\text{CO}_3/\text{BC}$, and $\text{H}_2\text{SO}_4/\text{BC}$, an inverse of this trend was observed ($\text{Zn}^{2+} > \text{Cd}^{2+} > \text{Mg}^{2+}$).

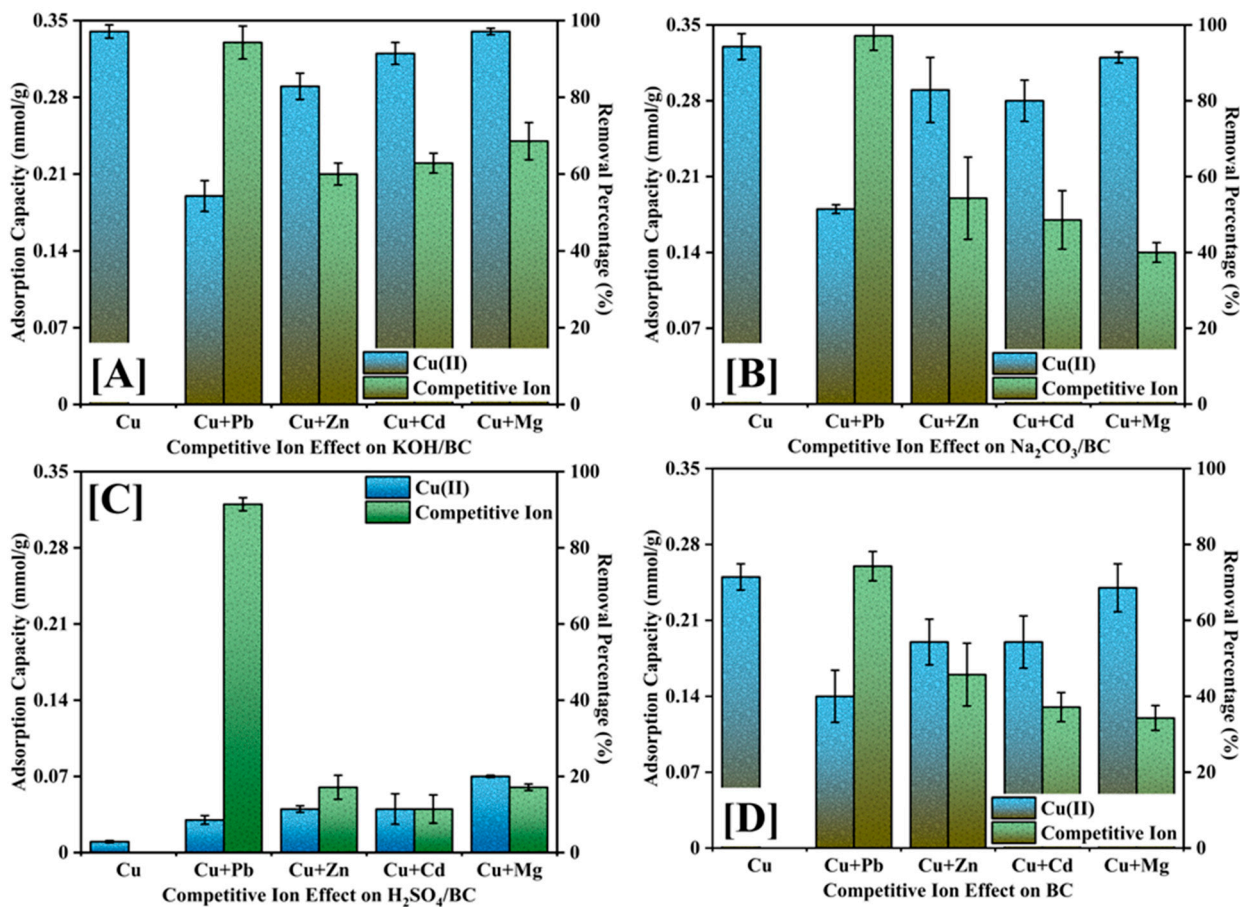


Figure 9. Effect of competitive ions (Pb²⁺, Zn²⁺, Cd²⁺, and Mg²⁺) on the uptake of Cu²⁺, where the Cu²⁺ and competitive ion concentrations were 0.7 mM, on (A) KOH/BC, (B) Na₂CO₃/BC, (C) H₂SO₄/BC, and (D) BC.

3.10. Effect of Real Water Matrices

It is evident from the data that Na₂CO₃/BC is more efficient at removing Cu²⁺ from aqueous solutions (Figure 10).

The removal percentages of Cu²⁺ were 95.5, 72.45, and 98.03% in Bluff, Briar, and Loakfoma Lakes. Similarly, removal percentages of 93.64, 89.57, and 98.91% were observed for KOH/BC, and 96.79, 91.74, and 99.99% for Na₂CO₃/BC across Bluff, Briar, and Loakfoma Lakes. H₂SO₄/BC had the lowest percentage removal, of 69.99, 58.91, and 61.34% for Bluff, Briar, and Loakfoma Lake water samples, respectively. With the biochar variants, the highest removal percentage was achieved with the Loakfoma water samples, except in the case of H₂SO₄/BC. In contrast, the lowest removal percentages were observed with Briar water samples, regardless of the adsorbents. The low Cu²⁺ removal exhibited in the Briar water sample is likely due to competition for sorption sites on the adsorbent by Ca²⁺. The Ca²⁺ concentrations in lake water samples were 23,154, 5432, and 3944 mg L⁻¹, respectively, for Briar, Bluff, and Loakfoma water samples, (Table S1). The low removal percentage achieved by H₂SO₄/BC for all water samples confirms that Cu²⁺ competes with H⁺ for binding sites onto the adsorbent surface.

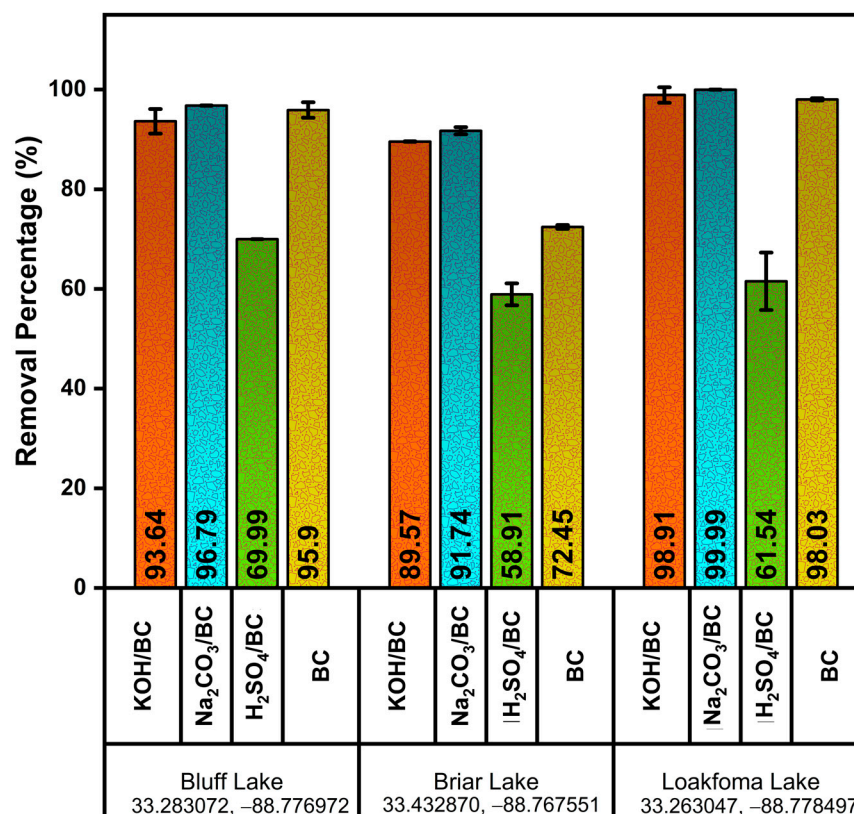


Figure 10. Removal percentages of Cu²⁺ in three different water matrices for KOH/BC, Na₂CO₃/BC, H₂SO₄/BC, and BC, respectively, at 2 mg/L initial Cu²⁺ concentrations.

4. Conclusions

Cu²⁺ removal from aqueous solution was investigated using Douglas fir biochar (BC) and BC modified with 20% solutions of KOH (KOH/BC), H₂SO₄ (H₂SO₄/BC), and Na₂CO₃ (Na₂CO₃/BC). Despite the modification, BC exhibited a higher specific surface area (578.9 m² g⁻¹) than KOH/BC (389.3 m² g⁻¹), Na₂CO₃/BC (367.9 m² g⁻¹), and H₂SO₄/BC (326.7 m² g⁻¹). The Cu²⁺ removal capacities were in the order Na₂CO₃/BC > KOH/BC > BC > H₂SO₄/BC, with maximum adsorption capacities of 24.79, 18.31, 18.21, and 9.17 mg g⁻¹, respectively. Cu²⁺ sorption from Loakfoma, Bluff, and Briar Lake water samples further demonstrated that Na₂CO₃/BC was more efficient than KOH/BC, BC, and H₂SO₄/BC. The corresponding Cu²⁺ removal percentages by Na₂CO₃/BC were 99.99, 96.79, and 91.74%, respectively, for Loakfoma, Bluff, and Briar Lake water samples. The percentages of removal by KOH/BC were 98.91, 98.03, and 93.64 and the removal percentage from BC were 95.9, 89.57 and 72.45%, for Loakfoma, Bluff, and Briar Lake water samples, respectively.

Supplementary Materials: The following supporting information can be downloaded at: <https://www.mdpi.com/article/10.3390/separations11030078/s1>, Figure S1: FTIR spectra of BC, KOH/BC, H₂SO₄/BC, and Na₂CO₃/BC; Figure S2: Thermogravimetric curve for BC, KOH/BC, Na₂CO₃/BC, and H₂SO₄/BC in nitrogen for temperature range from 25–1000 °C; Table S1: Initial physiochemical properties of Bluff, Briar, and Loakfoma lake water samples.

Author Contributions: B.A.: conceptualization, methodology, data analysis, writing original draft; P.M.R.: conceptualization, methodology, data analysis, writing original draft; O.A.O.: methodology, writing original draft; H.P.A.: methodology, writing original draft; J.N.T.: methodology; R.C.A.: conceptualization; T.E.M.: conceptualization, funding acquisition, review, and editing. All authors have read and agreed to the published version of the manuscript.

Funding: This work was supported by the USDA NIFA (361404) and Mississippi State University.

Data Availability Statement: Data is contained within the article and Supplementary Materials.

Acknowledgments: Mississippi State University, the Department of Chemistry, the Fulbright Organization, and the US Department of State are thanked for the scholarship awarded to Beatrice Arwenyo.

Conflicts of Interest: The authors declare no conflicts of interest.

References

1. Sulaiman, F.R.; Hamzah, H.A. Heavy metals accumulation in suburban roadside plants of a tropical area (Jengka, Malaysia). *Ecol. Process.* **2018**, *7*, 28. [[CrossRef](#)]
2. Boquete, M.T.; Lang, I.; Weidinger, M.; Richards, C.L.; Alonso, C. Patterns and mechanisms of heavy metal accumulation and tolerance in two terrestrial moss species with contrasting habitat specialization. *Environ. Exp. Bot.* **2021**, *182*, 104336. [[CrossRef](#)]
3. Taylor, A.A.; Tsuji, J.S.; Garry, M.R.; McArdle, M.E.; Goodfellow, W.L.; Adams, W.J.; Menzie, C.A. Critical review of exposure and effects: Implications for setting regulatory health criteria for ingested copper. *Environ. Manag.* **2020**, *65*, 131–159. [[CrossRef](#)] [[PubMed](#)]
4. Kerr, S.; Bonczek, R.; McGinn, C.; Land, M.; Bloom, L.; Sample, B.; Dolislager, F. *The Risk Assessment Information System*; Oak Ridge National Lab. (ORNL): Oak Ridge, TN, USA, 1998.
5. Shah, P.U.; Raval, N.P.; Shah, N.K. Adsorption of copper from an aqueous solution by chemically modified cassava starch. *J. Mater. Environ. Sci.* **2015**, *6*, 2573–2582.
6. Kavitha, C.; Vijayasarithi, P.; Tamizhdurai, P.; Mythily, R.M.R.; Mangesh, V.L. Retraction notice to “Elimination of Lead by Biosorption on Parthenium stem powder using Box-Behnken Design”. *S. Afr. J. Chem. Eng.* **2022**, *42*, 270–279. [[CrossRef](#)]
7. Râpă, M.; Țurcanu, A.A.; Matei, E.; Predescu, A.M.; Pantilimon, M.C.; Coman, G.; Predescu, C. Adsorption of copper (II) from aqueous solutions with alginate/clay hybrid materials. *Materials* **2021**, *14*, 7187. [[CrossRef](#)]
8. Martin, R. *Lead and Copper Rule Revisions: A Case Study in Identifying and Tracking Lead Water Service Lines with ArcGIS Field Maps*; The University of Arizona: Tucson, AZ, USA, 2022.
9. Qasem, N.A.; Mohammed, R.H.; Lawal, D.U. Removal of heavy metal ions from wastewater: A comprehensive and critical review. *Npj Clean. Water* **2021**, *4*, 36. [[CrossRef](#)]
10. Thompson, K.A.; Shimabuku, K.K.; Kearns, J.P.; Knappe, D.R.; Summers, R.S.; Cook, S.M. Environmental comparison of biochar and activated carbon for tertiary wastewater treatment. *Environ. Sci. Technol.* **2016**, *50*, 11253–11262. [[CrossRef](#)] [[PubMed](#)]
11. Lima, E.C. Removal of emerging contaminants from the environment by adsorption. *Ecotoxicol. Environ. Saf.* **2018**, *150*, 1–17.
12. Fuentes, A.L.B.; Arwenyo, B.; Nanney, A.L.; Ramirez, A.; Jamison, H.; Venson, B.; Mohan, D.; Mlsna, T.E.; Navarathna, C. Application of biochar for the removal of actinides and lanthanides from aqueous solutions. In *Sustainable Biochar for Water and Wastewater Treatment*, Elsevier: Amsterdam, The Netherlands, 2022; pp. 321–359.
13. Yaashikaa, P.; Kumar, P.S.; Varjani, S.; Saravanan, A. A critical review on the biochar production techniques, characterization, stability and applications for circular bioeconomy. *Biotechnol. Rep.* **2020**, *28*, e00570. [[CrossRef](#)]
14. Najim, T.S.; Elais, N.J.; Dawood, A.A. Adsorption of copper and iron using low cost material as adsorbent. *J. Chem.* **2009**, *6*, 161–168. [[CrossRef](#)]
15. Aydın, H.; Bulut, Y.; Yerlikaya, Ç. Removal of copper (II) from aqueous solution by adsorption onto low-cost adsorbents. *J. Environ. Manag.* **2008**, *87*, 37–45. [[CrossRef](#)]
16. Pavan Kumar, G.; Malla, K.A.; Yerra, B.; Srinivasa Rao, K. Removal of Cu (II) using three low-cost adsorbents and prediction of adsorption using artificial neural networks. *Appl. Water Sci.* **2019**, *9*, 44. [[CrossRef](#)]
17. Smith, M.; Ha, S.; Amonette, J.E.; Dallmeyer, I.; Garcia-Perez, M. Enhancing cation exchange capacity of chars through ozonation. *Biomass Bioenergy* **2015**, *81*, 304–314. [[CrossRef](#)]
18. Dewage, N.B.; Liyanage, A.S.; Pittman Jr, C.U.; Mohan, D.; Mlsna, T. Fast nitrate and fluoride adsorption and magnetic separation from water on α -Fe₂O₃ and Fe₃O₄ dispersed on Douglas fir biochar. *Bioresour. Technol.* **2018**, *263*, 258–265. [[CrossRef](#)] [[PubMed](#)]
19. Karunanayake, A.G.; Todd, O.A.; Crowley, M.; Ricchetti, L.; Pittman Jr, C.U.; Anderson, R.; Mohan, D.; Mlsna, T. Lead and cadmium remediation using magnetized and nonmagnetized biochar from Douglas fir. *Chem. Eng. J.* **2018**, *331*, 480–491. [[CrossRef](#)]
20. Rodrigo, P.M.; Navarathna, C.; Pham, M.T.; McClain, S.J.; Stokes, S.; Zhang, X.; Perez, F.; Gunatilake, S.R.; Karunanayake, A.G.; Anderson, R. Batch and fixed bed sorption of low to moderate concentrations of aqueous per- and poly-fluoroalkyl substances (PFAS) on Douglas fir biochar and its Fe₃O₄ hybrids. *Chemosphere* **2022**, *308*, 136155. [[CrossRef](#)] [[PubMed](#)]
21. Karunaratne, T.N.; Nayanathara, R.O.; Navarathna, C.M.; Rodrigo, P.M.; Thirumalai, R.V.; Pittman Jr, C.U.; Kim, Y.; Mlsna, T.; Zhang, J.; Zhang, X. Pyrolytic synthesis of graphene-encapsulated zero-valent iron nanoparticles supported on biochar for heavy metal removal. *Biochar* **2022**, *4*, 70. [[CrossRef](#)]
22. Chu, Y.; Zhu, S.; Wang, F.; Lei, W.; Xia, M.; Liao, C. Tyrosine-immobilized montmorillonite: An efficient adsorbent for removal of Pb²⁺ and Cu²⁺ from aqueous solution. *J. Chem. Eng. Data* **2019**, *64*, 3535–3546. [[CrossRef](#)]
23. Karunaratne, T.N.; Rodrigo, P.M.; Oguntuyi, D.O.; Mlsna, T.E.; Zhang, J.; Zhang, X. Unraveling biochar surface area on structure and heavy metal removal performances of carbothermal reduced nanoscale zero-valent iron. *J. Bioresour. Bioprod.* **2023**, *8*, 388–398. [[CrossRef](#)]

24. Aravamuthan, S.R.; Srinivasan, S.; Shukla, A.K. An in Situ Graphite-Grafted Alkaline Iron Electrode for Iron-Based Accumulators. In *ECS Meeting Abstracts*; IOP Publishing: Bristol, UK, 2013; p. 284.
25. Chai, W.S.; Cheun, J.Y.; Kumar, P.S.; Mubashir, M.; Majeed, Z.; Banat, F.; Ho, S.-H.; Show, P.L. A review on conventional and novel materials towards heavy metal adsorption in wastewater treatment application. *J. Clean. Prod.* **2021**, *296*, 126589. [[CrossRef](#)]
26. Behazin, E.; Ogunsona, E.; Rodriguez-Uribe, A.; Mohanty, A.K.; Misra, M.; Anyia, A.O. Mechanical, chemical, and physical properties of wood and perennial grass biochars for possible composite application. *BioResources* **2016**, *11*, 1334–1348. [[CrossRef](#)]
27. Zhang, C.; Zhang, N.; Xiao, Z.; Li, Z.; Zhang, D. Characterization of biochars derived from different materials and their effects on microbial dechlorination of pentachlorophenol in a consortium. *RSC Adv.* **2019**, *9*, 917–923. [[CrossRef](#)] [[PubMed](#)]
28. Siipola, V.; Tamminen, T.; Lahti, R.; Romar, H. Effects of Biomass Type, Carbonization Process, and Activated Carbons. *Bioresources* **2018**, *13*, 5976–6002. [[CrossRef](#)]
29. Huang, H.; Tang, J.; Gao, K.; He, R.; Zhao, H.; Werner, D. Characterization of KOH modified biochars from different pyrolysis temperatures and enhanced adsorption of antibiotics. *RSC Adv.* **2017**, *7*, 14640–14648. [[CrossRef](#)]
30. Rojas, R. Copper, lead and cadmium removal by Ca Al layered double hydroxides. *Appl. Clay Sci.* **2014**, *87*, 254–259. [[CrossRef](#)]

Disclaimer/Publisher’s Note: The statements, opinions and data contained in all publications are solely those of the individual author(s) and contributor(s) and not of MDPI and/or the editor(s). MDPI and/or the editor(s) disclaim responsibility for any injury to people or property resulting from any ideas, methods, instructions or products referred to in the content.